

Stripe dark solitons in a nonlinear optical fiber with second- and fourth-order dispersion

Peng Gao^{1,*}, Li-Zheng Lv², and Xin Li³

¹Graduate School, China Academy of Engineering Physics, Beijing 100193, China

²School of Physics, Xi'an Jiaotong University, Xi'an 710049, China and

³School of Science, Beijing University of Posts and Telecommunications, Beijing 100876, China

We study the soliton excitations in a nonlinear optical fiber with the second- and fourth-order dispersion, and find the emergence of stripe dark solitons (SDSs) in addition to the existing stripe bright solitons (SBSs). The SDSs can exhibit the fundamental structures and their counterparts without a phase step, as well as the compound structures with different numbers of humps. By the modified linear stability analysis, we regard the formation of fundamental SDS as the competition between its periodicity and localization, and analytically give its existence condition, oscillation frequency, and transmission stability, which show great agreements with numerical results. We also show good predictions for the characteristics of SBS, and find that SBS will become the pure-quartic soliton when its periodicity and localization keep balance. Our results can be observable with current experimental techniques in nonlinear optical fibers, and our method can also guide the discovery of stripe solitons in other physical systems.

PACS numbers:

I. INTRODUCTION

Periodicity and localization are two fundamental but distinct characteristics of nonlinear waves. The periodicity is a commonality of all waves and dominates various wave phenomena [1, 2], while the (self-induced) localization dominates the formation of nonlinear localized waves [3–6]. As a kind of localized wave broadly existing in nonlinear physical systems, soliton has been attracting lots of attentions and has wide applications by virtue of its property of stable propagation [7–11]. Soliton can produce periodicity-dominated phenomena like interference [11–13] and diffraction [14, 15], and it also has localization-dominated phenomena like self-bound propagation and elastic collision [16, 17]. In the previous studies, the periodicity and localization of a soliton were always treated separately, and little attention has been paid to their combined effects. However, in nonlinear fibers with the fourth-order dispersion (FOD), the bright solitons with oscillating tails [18–21] and even stripe structures [22, 23] were discovered, which are the manifestation of the competition between periodicity and localization. Therefore, to figure out the formation mechanism of these solitons and find more kinds of solitons in this system, it is necessary to quantify the two characteristics and analyze the competition between them.

In this paper, we study the soliton excitations in a nonlinear optical fiber with the second-order dispersion and FOD. We find that stripe dark solitons (SDSs) exist in this system and have more interesting structures than the stripe bright solitons (SBSs) shown in Refs. [22, 23]. These structures contains the fundamental SDSs and their counterparts without a phase step, as well as the compound structures with different numbers of humps. By the modified linear stability analysis (MLSA) method [24, 25], a fundamental SDS is considered as the result of the competition between periodicity and localization, and furthermore we quantitatively give its existence con-

dition and oscillation frequency. Based on the derived oscillation frequency, we analyze the modulation instability (MI) of SDSs and give its stability condition. Besides, we apply the MLSA to the SBSs to give a more accurate prediction for their oscillation frequency, and find that the pure-quartic soliton is a special kind of SBS when its periodicity and localization keep balance.

II. MODEL AND THE EXISTENCE CONDITION OF STRIPE SOLITONS

In the slow-varying envelope approximation, the propagation of a linearly polarized light in a single-mode nonlinear fiber can be described by the following nonlinear Schrödinger equation with the second-order dispersion and FOD [8],

$$i \frac{\partial A}{\partial Z} - \frac{\beta'_2}{2} \frac{\partial^2 A}{\partial T^2} + \frac{\beta'_4}{24} \frac{\partial^4 A}{\partial T^4} + \gamma |A|^2 A = 0, \quad (1)$$

where $A(T, Z)$ represents the slowly varying complex envelope of optical field, and Z, T are the evolution distance and retarded time. β'_2, β'_4 , and γ are the coefficients of second-order dispersion, FOD, and Kerr nonlinearity, respectively. By the transformation $A = \sqrt{P_0} \psi$, $Z = U_z z$, and $T = U_t t$, the model (1) can be transformed into a dimensionless model,

$$i \frac{\partial \psi}{\partial z} - \frac{\beta_2}{2} \frac{\partial^2 \psi}{\partial t^2} + \frac{\beta_4}{24} \frac{\partial^4 \psi}{\partial t^4} + |\psi|^2 \psi = 0, \quad (2)$$

where $\beta_2 = \beta'_2 U_z / U_t^2$, $\beta_4 = \beta'_4 U_z / U_t^4$, and P_0 is the background value of the incident light power. The two quantities, U_z and U_t , respectively have the units of space and time. In Ref. [26], to generate a pure-quartic soliton in a fiber laser, the parameters were set as $\beta'_2 = 21.4 \text{ ps}^2/\text{km}$, $\beta'_4 = -80 \text{ ps}^4/\text{km}$, $\gamma = 1.6/\text{W}/\text{km}$, and $P_0 = 0.37 \text{ W}$. When $U_z = 1/\gamma P_0 = 1.69 \text{ km}$ and $U_t = 6 \text{ ps}$, one can obtain $\beta_2 = 1$ and $\beta_4 = -0.13$. In our work, the range of β_2 and β_4 will be extended to generate more kinds of solitons.

*Electronic address: pgao@gascaep.ac.cn

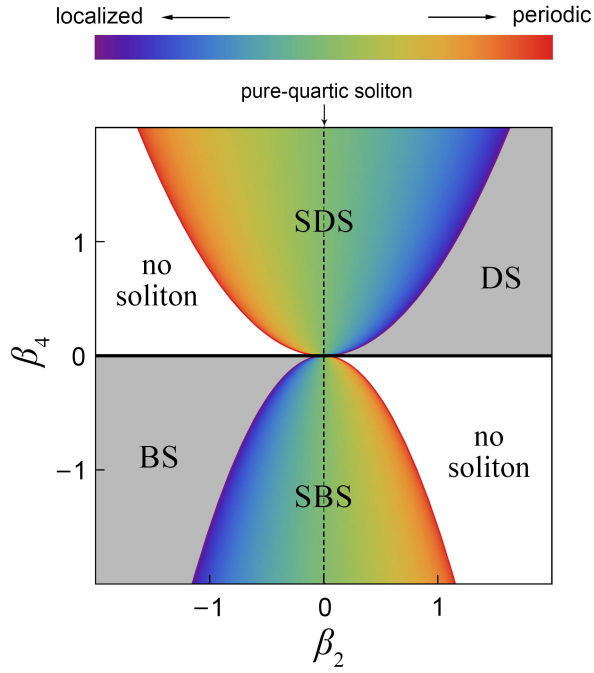


FIG. 1: (Color online) Existence condition of solitons under different second-order dispersion β_2 and FOD β_4 . They contain the regions of SDS (stripe dark soliton), DS (the traditional dark soliton), SBS (the stripe bright soliton), and BS (the traditional bright soliton). The boundary of SDS region has the expression $\beta_4 = 3\beta_2^2/4a_0^2$, and the boundaries of SBS region is $\beta_4 = -3\beta_2^2/2\beta$, where a_0 and β are respectively the SDS's background amplitude and the SBS's propagation constant. The color scale describes the strength φ of a soliton's periodicity relative to its localization in the range from 0 to $\pi/2$. The black dashed line denotes the case of $\beta_2 = 0$, where a pure-quartic soliton can exist. The parameters are set as $a_0 = \beta = 1$.

The existence condition of solitons in the model (2) is shown in Fig. 1. Different kinds of solitons correspond to different regions in the β_2 - β_4 plane. The details are as follows.

- When $\beta_4 = 0$, the model (2) becomes the standard nonlinear Schrödinger model, where only the traditional dark ($\beta_2 > 0$) or bright ($\beta_2 < 0$) solitons can exist.
- When $\beta_4 > 3\beta_2^2/4a_0^2$, the SDSs exist and their periodicity gets stronger with β_2 decreasing [see Eq. (15)].
- When $\beta_4 \leq 3\beta_2^2/4a_0^2$ and $\beta_2 > 0$, the traditional dark soliton exists, which has no stripe.
- When $\beta_4 < -3\beta_2^2/2\beta$, the SBSs exist and their periodicity gets stronger with β_2 increasing [see Eq. (25)]. In particular, it becomes the so-called pure-quartic soliton when $\beta_2 = 0$ [20].
- When $\beta_4 < -3\beta_2^2/2\beta$ and $\beta_2 < 0$, the traditional bright soliton exists, which has no stripe.

In the above conditions, $a_0 (> 0)$ denotes the plane-wave background's amplitude of dark solitons, and $\beta (> 0)$ denotes the

propagation constant of bright solitons. In other regions of the β_2 - β_4 plane, no soliton exists. We define the quantity φ by $\varphi = \tan^{-1}(\omega_s/\eta_s)$ in the range from 0 to $\pi/2$ to describe the strength of a wave's stripe characteristic. ω_s and η_s are respectively the parameters determining the periodicity and localization of a wave, whose expressions can be seen in Eqs. (14) and (24) for SDS and SBS, respectively. With φ increasing, the wave's periodicity gets stronger and the wave's localization gets weaker. The stripe solitons with different shapes can be regarded as the results of the competition between periodicity and localization in different proportions. In particular, for a pure-quartic soliton [20], the two parameters ω_s and η_s are equal, which indicates that its periodicity and localization keep balance.

In the next two sections, we will separately study SDS and SBS, including their existence condition, stripe characteristic, and formation mechanism.

III. SDS

In the model (2), we find two major kinds of SDSs, which severally have the fundamental and compound structures. At first, let us focus on the SDSs with fundamental structures and their counterparts without a phase step. Considering that it is quite difficult to analytically solve Eq. (2), we numerically solve it by the biconjugate gradient method [27]. This numerical method has been successfully applied to obtain dark solitons or vortices in different models of Bose-Einstein condensates [28, 29]. By this method, when $\beta_4 = 1$, we obtain the numerical solutions of dark solitons under different β_2 and show them in Fig. 2. When $\beta_2 = -1$, we find two kinds of fundamental SDSs, which has or does not have a phase step (i.e., the key characteristic of dark solitons), and we show them at the top or bottom of Fig. 2 (a), respectively. Both of them have some stripes and oscillating tails, but their structures are different. Later, we set their wave functions as the initial states to numerically integrate the model (2), by the split-step Fourier method [30]. The evolution results are shown as the insets in Fig. 2 (a). The SDS with the phase step stably propagates for seven unit distance. At its final evolution stage, some new waves can be seen, which is generally induced by the modulation instability (MI). The similar result is also obtained for the SDS without a phase step, which propagates stably for six unit distance.

For some larger values of β_2 , the results are shown in Figs. 2 (b), (c), (d), and (e). The SDS has less stripes but can propagate for a longer distance, especially when $\beta_2 > 0$. Note that the SDS without a phase step can be regarded as two separated dark solitons when $\beta_2 = 1.5$, as shown in Fig. 2 (e). It indicates that, when the SDS dose not exist, there will not exist the dark soliton without a phase step.

As shown in Fig. 2, the SDSs have both of periodicity and localization. For such a nonlinear wave, the MLSA method can quantitatively give its dynamical characteristics and guide its generation [24, 25]. Thus, we will apply this method to analyze the existence condition and characteristics of fundamental SDSs. It starts with the ansatz solution of a perturbed

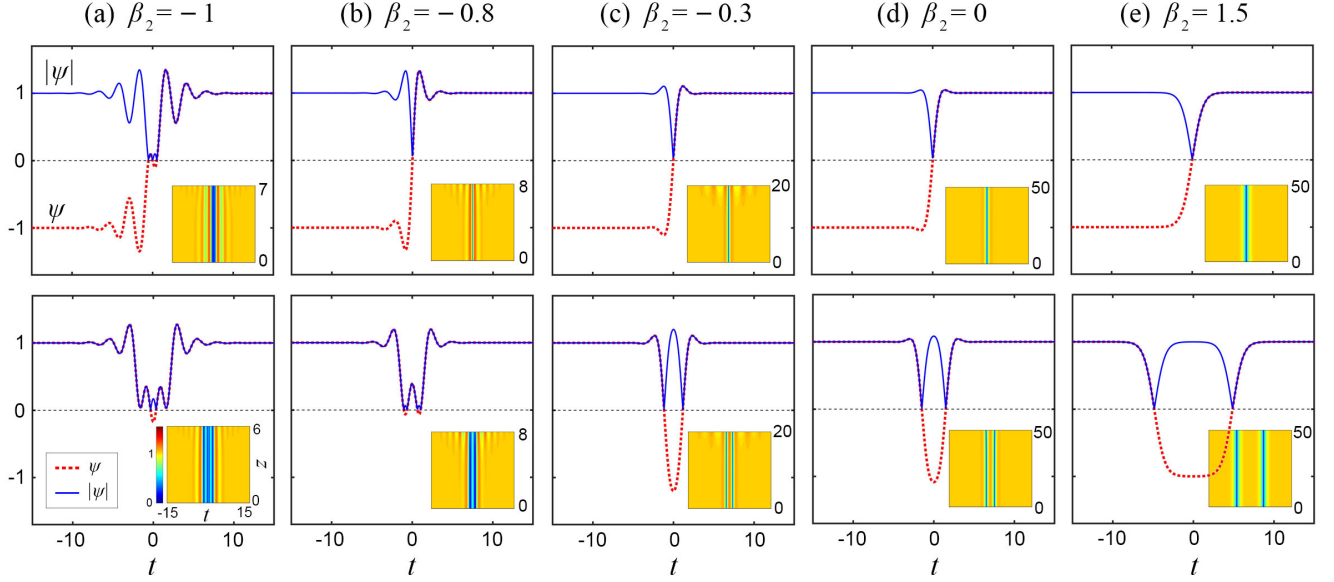


FIG. 2: (Color online) Distributions of the wave functions ψ of dark solitons (red dashed curves) and their amplitude $|\psi|$ (blue solid curves), when the second-order dispersion β_2 is (a) -1 , (b) -0.8 , (c) -0.3 , (d) 0 , and (e) 1.5 . The upper and lower rows are the dark solitons with and without a phase step, respectively. The insets are their corresponding amplitude evolution plots. Other parameters are set as $\beta_4 = 1$ and $a_0 = 1$.

plane wave,

$$\psi_p = \psi_0(1 + u), \quad (3)$$

where $\psi_0 = a_0 e^{i a_0 z}$ is a plane wave with the amplitude a_0 , and u denotes a perturbation exerted on it. Substituting Eq. (3) into the model (2) and linearizing it about u , we can obtain

$$i \frac{\partial u}{\partial z} - \frac{\beta_2}{2} \frac{\partial^2 u}{\partial t^2} + \frac{\beta_4}{24} \frac{\partial^4 u}{\partial t^4} + a_0^2 (u + u^*) = 0, \quad (4)$$

where u^* denotes the complex conjugation of u . Then, we assume the perturbation as the linear superposition of two conjugating components,

$$u = A e^{p(t,z)} + B e^{p^*(t,z)}, \quad (5)$$

where A and B are the complex amplitude of the two components, and $p(t,z)$ is a complex function. Substituting Eq. (5) into the perturbation's model (4) and only considering the parts of $e^{p(t,z)}$, one can obtain two linear equations about A and B^* . The condition that the equations have non-zero solutions is

$$p_z = \sqrt{M(2a_0^2 - M)}, \quad (6)$$

where

$$M = \frac{\beta_2}{2} p_{tt} - \frac{\beta_4}{24} p_t^4 - \frac{\beta_4}{8} p_{tt}^2 - \frac{\beta_4}{6} p_t p_{ttt} - \frac{\beta_4}{24} p_{tttt} - p_t^2 \left(-\frac{\beta_2}{2} + \frac{\beta_4}{4} p_{tt} \right). \quad (7)$$

In the above expressions, p_t and p_z denote the partial deriva-

tive of $p(t,z)$ about t and z , respectively.

Now, our main aim is to find the condition that the shape of the perturbation remains unchanged in the propagating process, which is just the existence condition of SDS. We consider the function $p(t,z)$ has the following form at the initial distance,

$$p(t, z = 0) = i\omega t + \ln[\text{sech}(\eta t)], \quad (8)$$

where ω and η are the perturbation's frequency and steepness, determining its periodicity and localization, respectively. The localized function with the sech form is set because it has the following limit value,

$$p_t^{(\pm)} = \lim_{t \rightarrow \pm\infty} p_t = i\omega \mp \eta. \quad (9)$$

By this limit, the function $p_t(t,z)$ can be successfully transformed into a complex constant, and therefore offers great convenience for our analysis. Moreover, this limit can be conveniently applied to the function p_z and produce

$$p_z^{(-)} = \sqrt{M^{(-)}(a_0^2 - M^{(-)})}, \quad (10)$$

where

$$M^{(-)} = (i\omega + \eta)^2 \left[\frac{\beta_2}{2} - \frac{\beta_4}{24} (i\omega + \eta)^2 \right]. \quad (11)$$

It describes the propagating characteristics of the perturbation. To be specific, the perturbation's propagation constant and growing rate relative to the plane wave are respectively

$$K = \text{Im}[p_z^{(-)}], \quad G = \text{Re}[p_z^{(-)}]. \quad (12)$$

Then, the velocity of its localized envelope and stripes are

$$V_{\text{en}} = G/\eta, \quad V_{\text{st}} = K/\omega. \quad (13)$$

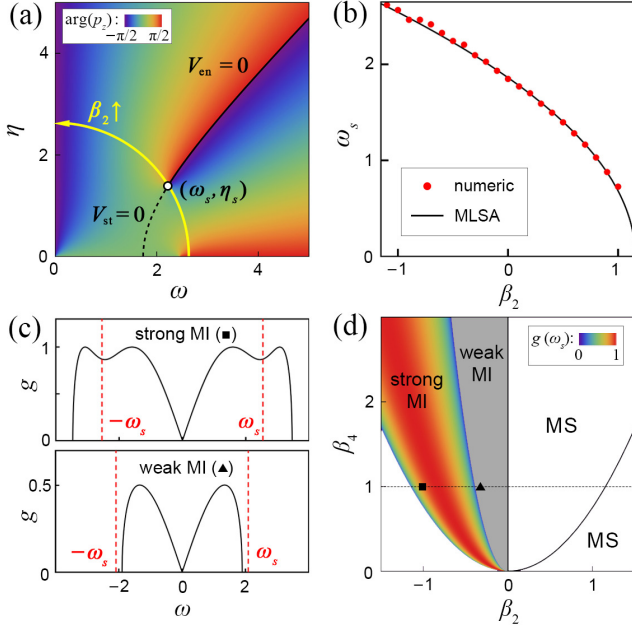


FIG. 3: (Color online) (a) Phase of the propagating function $p_z(t, z)$ under different ω and η , when $\beta_2 = -0.5$, $\beta_4 = 1$, and $a_0 = 1$. The black solid and dashed curves denote $V_{\text{en}} = 0$ and $V_{\text{st}} = 0$, respectively. The white point with the coordinate (ω_s, η_s) is an exceptional point of $\arg(p_z)$ function. The yellow curve with an arrow is the trajectory of this point with β_2 increasing. (b) Dependence of SDS's oscillation frequency ω_s on β_2 , when $\beta_4 = 1$. The red dots and the black curve are respectively the results from numerical evolution and the MLSA method. (c) Dependence of the gain value G on ω , when $\beta_2 = -1$ (upper) or $\beta_2 = -0.3$ (lower). The strong or weak MI is defined by whether ω_s locates in the MI band or not. (d) MI and MS distribution on the β_2 - β_4 plane. The color scale describes the value of $g(\omega_s)$.

From the insets of Fig. 2, we know that a SDS has a zero-velocity localized envelope and some zero-velocity stripes, which indicates $V_{\text{en}} = 0$ and $V_{\text{st}} = 0$. In Fig. 3 (a), when $\beta_2 = -0.5$, $\beta_4 = 1$, and $a_0 = 1$, we show the curves of $V_{\text{en}} = 0$ and $V_{\text{st}} = 0$ in the ω - η plane. The coordinate of their intersection point (ω_s, η_s) is just the oscillation frequency and steepness of SDS, and the expressions are

$$\begin{aligned} \omega_s &= \text{Re}\left[\sqrt{\frac{-3\beta_2 + 2\sqrt{3}a_0\sqrt{\beta_4}}{\beta_4}}\right], \\ \eta_s &= \text{Re}\left[\sqrt{\frac{3\beta_2 + 2\sqrt{3}a_0\sqrt{\beta_4}}{\beta_4}}\right]. \end{aligned} \quad (14)$$

Thus, the parameters need to satisfy $\omega_s \neq 0$ and $\eta_s \neq 0$ for the existence of SDS, namely

$$\beta_4 > 3\beta_2^2/4a_0^2, \quad (15)$$

as shown in Fig. 1. Besides, one can find that they have the relationship,

$$\omega_s^2 + \eta_s^2 = \frac{4\sqrt{3}a_0}{\sqrt{\beta_4}}, \quad \omega_s^2 - \eta_s^2 = -\frac{6\beta_2}{\beta_4}. \quad (16)$$

The former is independent of β_2 , and the latter is independent of a_0 . Thus, the point (ω_s, η_s) always locates on a circle when β_4 and a_0 are fixed, and it moves towards the positive axis of η with β_2 increasing, as shown in Fig. 3 (a). More interestingly, this point is just an exceptional point of the phase of p_z , and its winding number is π . However, for the relationship between SDS and exceptional points, a deeper understanding needs further investigations. Next, to verify the effectiveness of our prediction, the dependence of ω_s on β_2 is studied. When $\beta_4 = 1$ and $a_0 = 1$, we numerically measure the oscillation frequency of SDSs under different values of β_2 and show them by the red dots in Fig. 3 (b). One can see that ω_s gradually decreases into 0 with β_2 increasing. To obtain them, we measure the time interval between the first and second peaks on the right side of SDS as its time period T_s , and then the oscillation frequency can be calculated by $\omega_s = 2\pi/T_s$. On the other hand, we also show the analytic prediction from the MLSA method by the black curve. There are great agreements between the two results.

Another problem worthy of consideration is the transmission stability of SDSs. From the insets of Fig. 2, one can see that some spontaneous oscillations emerge in the propagating process of SDSs, which is a widespread phenomenon in the nonlinear systems with MI. It prompts us to analyze the MI in the model (2). As we know, different types of perturbations can produce different phenomena under the influence of MI. Generally speaking, a purely periodic perturbation can generate Akhmediev breathers [6, 31]; a purely localized one can generate a rogue wave [32] or Kuznetsov-Ma breather [33], and induce the spontaneous oscillations in a triangular region [34, 35]. (The word "purely" in front of "perturbation" is used to distinguish them with a periodic-localized perturbation.) A SDS at the initial distance can be seen as a periodic-localized perturbation on a plane wave, so we need to separately consider the influence of MI on its periodic and localized components. For its periodic component, we know that the traditional growing rate g can be obtained by the modified growing rate G when $\eta = 0$, namely

$$\begin{aligned} g(\omega) &= G(\omega, \eta = 0) \\ &= \omega^2 \left(\frac{\beta_2}{2} + \frac{\beta_4}{24} \omega^2 \right) \left(2a_0^2 + \frac{\beta_2}{2} \omega^2 + \frac{\beta_4}{24} \omega^4 \right). \end{aligned} \quad (17)$$

If the SDS's oscillation frequency ω_s locates in the MI band, its periodicity will impact the stability of perturbation, whose corresponding MI distribution is shown as the upper plot in Fig. 3 (c). Thus, we calculate the growing rate when $\omega = \omega_s$ by

$$g(\omega_s) = \frac{(3\beta_2^2 - 4a_0^2\beta_4)(-27\beta_2^2 + 24\sqrt{3}a_0\beta_2\sqrt{\beta_4} + 20a_0^2\beta_4)}{64\beta_4^2}, \quad (18)$$

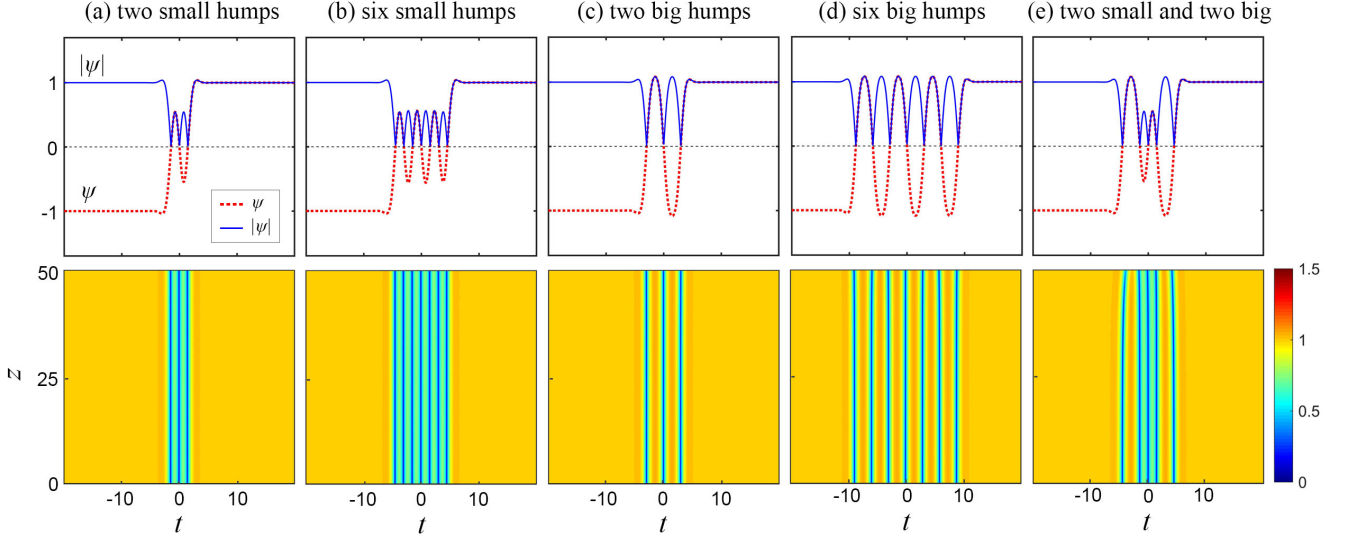


FIG. 4: (Color online) The SDSs with compound structures. The upper row is the distribution of their wave functions ψ (red dashed curves) and amplitude $|\psi|$ (blue solid curves), when $\beta_2 = 0$, $\beta_4 = 1$, and $a_0 = 1$. The lower row is their corresponding amplitude evolution.

to describe the MI growing rate induced by the periodicity. Because it can produce MI phenomena faster than the localization component, we call the periodicity-induced MI "strong MI", and accordingly we call the localization-induced MI "weak MI". The typical distribution of growing rate of weak MI is shown as the lower plot in Fig. 3 (c). In Fig. 3 (d), we illustrate the phase diagram of strong MI, weak MI, and modulation stability (MS) on the β_2 - β_4 plane, and the growing rate of strong MI is presented by the color scale. The strong MI corresponds to the region of $\beta_2 < 0$ and $\frac{3\beta_2^2}{4a_0^2} < \beta_4 < \frac{27\beta_2^2}{4a_0^2}$, and the weak MI is in the region of $\beta_2 < 0$ and $\beta_4 > \frac{27\beta_2^2}{4a_0^2}$. When $\beta_4 = 1$, the strong and weak MI respectively need the conditions of $-2/\sqrt{3} < \beta_2 < -2/9$ and $\beta_2 > -2/9$. It is consistent with the evolution plots in Fig. 2, where the SDS is more and more stable with β_2 increasing.

Besides of the fundamental structures shown above, we also find some SDSs with compound structures. When $\beta_2 = 0$, $\beta_4 = 1$, and $a_0 = 1$, the distributions of wave functions of SDSs with compound structures are shown as the upper row in Fig. 4. There are many kinds of compound structures, which have different number of humps, like (a) two small humps, (b) six small humps, (c) two big humps, (d) six big humps, and (e) two small and two big humps. The compound structures of SDS include but are not limited to these five kinds. Their counterparts without a phase step also exist but are not shown in this paper. Next, we study their numerical evolution to test their transmission stability, which are shown as the lower row in Fig. 4. The SDSs with compound structures can always propagate for a long distance, and no MI phenomenon emerges.

IV. SBS

As we know, the bright soliton with stripe structures in the model (2) has been studied in Refs. [22, 23], including their existence condition and oscillation frequency. Here, we will study them by the MLSA method to provide a more accurate prediction for their characteristics and our understanding of their formation mechanism.

Firstly, by the biconjugate gradient method, we show the distribution of wave functions of SBS in Fig. 5 (a) when $\beta_2 = 0$, $\beta_4 = -1$, and the propagation constant $\beta = 1$. A bright soliton with oscillating tails can be seen, which is just the so-called pure-quartic soliton. Then, when we change β_2 to 0.75, a bright soliton with many stripes appear. Unlike the SDS, the SBS do not have the background of plane wave. Thus, our calculation of MLSA directly starts with the perturbation,

$$\psi_p = u = Ae^{p(t,z)} + Be^{p^*(t,z)}, \quad (19)$$

where the function $p(t,z)$ still has the form of Eq. (8) at the initial distance. Then, substituting Eq. (19) into the model (2) and considering that the perturbation has a small amplitude, one can obtain

$$p_z = i\{p_t^2[-\frac{\beta_2}{2} + \frac{\beta_4}{24}(p_t^2 + p_{tt})] + p_{tt}(-\frac{\beta_2}{2} + \frac{\beta_4}{8}p_{tt}) + \frac{\beta_4}{6}p_t p_{ttt} + \frac{\beta_4}{24}p_{tttt}\}. \quad (20)$$

After taking the limitations of $t \rightarrow -\infty$, the propagation function becomes

$$p_z^{(-)} = i(i\omega + \eta)^2[-\frac{\beta_2}{2} + \frac{\beta_4}{24}(i\omega + \eta)^2]. \quad (21)$$

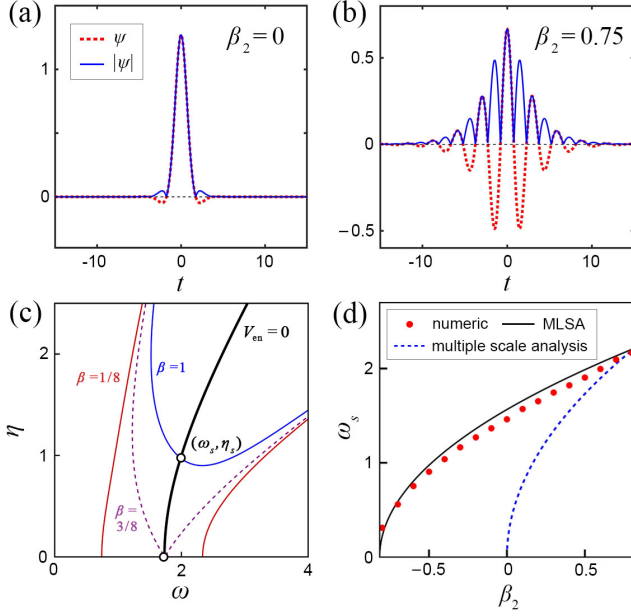


FIG. 5: (Color online) (a) Distribution of the SBS's wave function ψ (red dashed curves) and their amplitude $|\psi|$ (blue solid curves), when $\beta_2 = 0$, $\beta_4 = -1$ and $\beta = 1$. (b) Same as (a) except for $\beta_2 = 0.75$. (c) In the ω - η plane, the characteristic parameters (ω_s, η_s) is the intersection point between the curves of $V_{\text{en}} = 0$ (black solid curve) and different β value. The blue solid, purple dashed, and red solid curves denote $\beta = 1, 3/8$, and $1/8$, respectively. The parameters are $\beta_2 = 0.5$ and $\beta_4 = -1$. (d) Dependence of SBS's oscillation frequency ω_s on β_2 , when $\beta_4 = 1$ and $\beta = 1$. The red dots, the black solid curve, and the dashed blue curve are respectively the results of numerical solutions, the MLSA method [see Eq. (24)], and the multiple scale analysis giving the expression $\omega_s = \sqrt{6\beta_2/|\beta_4|}$.

It indicates that the propagation constant of this wave is

$$\beta = \text{Im}[p_z^{(-)}] = -\frac{\beta_2}{2}(\eta^2 - \omega^2) + \frac{\beta_4}{24}[(\eta^2 - \omega^2)^2 - 4\omega^2\eta^2]. \quad (22)$$

It is worth noting that the formation mechanism of stripes in SDS and SBS is different. For SDS, the stripes originate from the interaction between a perturbation and a zero-velocity plane wave; for SBS, the stripes are caused by the interaction between two components with opposite frequencies. Thus, the velocity of stripes in SBS is not equal to $V_{\text{st}} = K/\omega$. On the other hand, the formation of localized envelopes is not related to the background wave, so V_{en} can still describe the velocity of localized envelopes in SBS. Its expression is

$$V_{\text{en}} = G/\eta = \text{Re}[p_z^{(-)}]/\eta = \omega[\beta_2 + \frac{\beta_4}{6}(\omega^2 - \eta^2)]. \quad (23)$$

For a certain propagation constant β , by solving $V_{\text{en}} = 0$ and Eq. (22), we can obtain that the oscillation frequency and

steepness of SBS,

$$\omega_s = \text{Re}\left[\sqrt{\frac{3\beta_2 + \sqrt{-6\beta\beta_4}}{-\beta_4}}\right],$$

$$\eta_s = \text{Re}\left[\sqrt{\frac{-3\beta_2 + \sqrt{-6\beta\beta_4}}{-\beta_4}}\right]. \quad (24)$$

As shown in Fig. 5, the point (ω_s, η_s) is the intersection of the black curve ($V_{\text{en}} = 0$) and the blue curve ($\beta = 1$), when $\beta_2 = 0.5$ and $\beta_4 = -1$. We also depict the curves of $\beta = 3/8$ and $\beta = 1/8$: the former is the critical case where the intersection exists just right, and the latter has no intersection with the curve of $V_{\text{en}} = 0$. It indicates that the SBS cannot exist when $\beta < 3/8$, and we also obtain the same result in our numerical simulations. Then, considering that $\omega_s \neq 0$ and $\eta_s \neq 0$, we can obtain that the existence condition of SBS is

$$\beta_4 < -3\beta_2^2/2\beta, \quad (25)$$

as shown in Fig. 1. We also show the oscillation frequency of SDS under different sets of β_2 in Fig. 5 (d), when $\beta_4 = 1$ and $\beta = 1$. There are the results from three approaches, i.e., the numerical solutions, the MLSA method [see Eq. (24)], and the multiple scale analysis in Ref. [23] giving the expression $\omega_s = \sqrt{6\beta_2/|\beta_4|}$. The MLSA method shows a better agreement with numerical results than the multiple scale analysis.

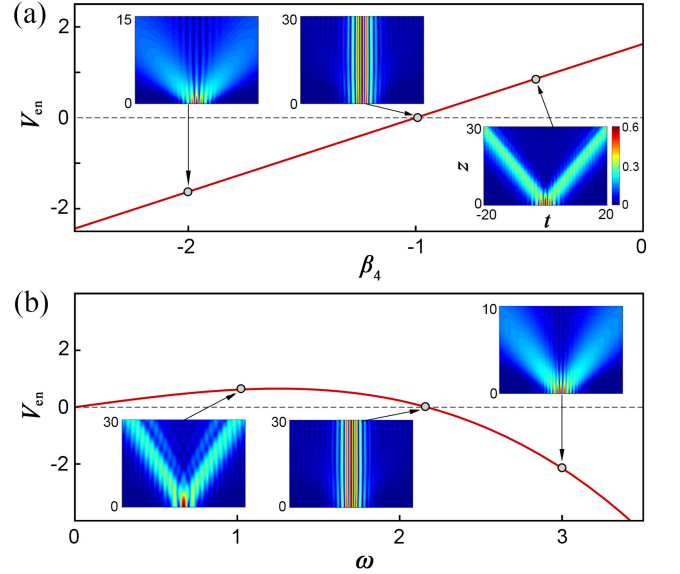


FIG. 6: (Color online) (a) Dependence of V_{en} on β_4 when $\omega = 2.1678$, $\eta = 0.4466$, and $\beta_2 = 0.75$. The insets are the amplitude evolution of the initial state when $\beta_4 = -2, -1$, and -0.5 . (b) Dependence of V_{en} on ω when $\eta = 0.4466$, $\beta_2 = 0.75$, and $\beta_4 = -1$. The insets are the amplitude evolution of the initial state when $\omega = 1, 2.1678$, and 3 .

The wave function (19) has two components with opposite frequencies. When both of their localized envelopes have the zero velocity, i.e., $V_{\text{en}} = 0$, a SBS will be generated, which can

TABLE I: Characteristics of different nonlinear waves

	Periodicity (ω_s)	Localization (η_s)	Proportion (ω_s/η_s)	Characteristic quantity (φ)
Traditional soliton	No ($\omega_s = 0$)	Yes ($\eta_s > 0$)	0	0
Stripe soliton	Yes ($\omega_s > 0$)	Yes ($\eta_s > 0$)	$(0, +\infty)$	$(0, \pi/2)$
Pure-quartic soliton	Yes ($\omega_s > 0$)	Yes ($\eta_s > 0$)	1	$\pi/4$
Periodic wave	Yes ($\omega_s > 0$)	No ($\eta_s = 0$)	$+\infty$	$\pi/2$

be considered as the result of synchronous transmission of the two components. To confirm our guess, for a wave function with frequency ω and steepness η , we show the dependence of V_{en} on β_4 in Fig. 6 (a), when $\omega = 2.1678$, $\eta = 0.4466$, and $\beta_2 = 0.75$. When $\beta_4 = -1$, we have $V_{\text{en}} = 0$. The initial state has the form of

$$\psi(t, 0) = a \cos(\omega t) \text{sech}(\eta t), \quad (26)$$

where the amplitude a is set as 0.6 according to the numerical solution of the SBS in this case. Its amplitude evolution plot is shown in the middle inset of Fig. 6 (a), where a SBS is generated. When $\beta_4 = -2$, we have $V_{\text{en}} < 0$. Its corresponding evolution plot is shown in the left insets of Fig. 6 (a), where the two components move towards opposite directions. Also, the similar result can be obtained in the case of $\beta_4 = -0.5$, as shown in the right inset. It indicates that one cannot find SBS in the absence of FOD, because the velocity of localized envelopes is not zero in this case.

Similarly, we also show the dependence of V_{en} on ω in Fig. 6 (b), when $\eta = 0.4466$, $\beta_2 = 0.75$, and $\beta_4 = -1$. The evolution plots in the cases of $\omega = 1$, 2.1678, and 3 are shown as the insets in Fig. 6. Only in the case of $\omega = 2.1678$, the SBS can be generated. In the cases of $\omega \neq 2.1678$, the two components propagate towards opposite directions.

Finally, we summary the characteristics of different nonlinear waves in Tab. I. They contains the traditional solitons, the stripe solitons, the pure-quartic solitons, and periodic waves. We recall that the quantity φ is defined by $\varphi = \tan^{-1}(\omega_s/\eta_s)$ to describe the strength of a wave's periodicity relative to its localization, and ω_s and η_s are the parameters determining the periodicity and localization of a wave, respectively. A traditional soliton has the localization but no the periodicity (i.e., $\omega_s = 0$ and $\eta_s > 0$), while a periodic wave has the periodicity but no the localization (i.e., $\omega_s > 0$ and $\eta_s = 0$). A stripe soliton has both of the periodicity and localization, and therefore it corresponds to $\omega_s > 0$ and $\eta_s > 0$. The

pure-quartic soliton is a particular case of the stripe solitons when the periodicity and localization achieve a balance, i.e., $\omega_s = \eta_s$, so its proportion of periodicity and localization is $\omega_s/\eta_s = 1$ and the characteristic quantity is $\varphi = \pi/4$.

V. CONCLUSION

In summary, the SDSs in nonlinear fibers with the second-order dispersion and FOD are investigated. The SDSs have the fundamental structures, their counterpart without a phase step, and some compound structures with different numbers of humps. With the help of the MLSA method, we quantitatively analyze the periodicity and localization of fundamental SDSs under different coefficients of second-order dispersion and FOD. Their oscillation frequency is successfully predicted and the corresponding MI is analyzed. For the SBSs, though their major characteristics have been studied in the previous works [22, 23], we provide a new perspective to understand their formation mechanism and show a more accurate prediction of their oscillation frequency. Our method and results can provide the theoretical guidance for the generations and manipulations of stripe solitons in nonlinear fibers, and furthermore bring more possibility for their applications in soliton communications and optical measurements. Considering that stripe solitons have been also found in spinor Bose-Einstein condensates [36–39], we expect that our method can be applied in these systems and help with the observation of matter-wave stripe solitons.

Acknowledgement

The authors thank Prof. Jie Liu for their helpful discussions. This work was supported by NSAF (No.U2330401) and National Natural Science Foundation of China (No. 12247110).

[1] E. Hecht, Optics (Addison-Wesley, Reading, MA, 2001).
[2] A. D. Cronin, J. Schmiedmayer, and D. E. Pritchard, Optics and interferometry with atoms and molecules, Rev. Mod. Phys. 81, 1051 (2009).
[3] L. F. Mollenauer, R. H. Stolen, and J. P. Gordon, Experimental observation of picosecond pulse narrowing and solitons in

optical fibers, Phys. Rev. Lett. 45, 1095 (1980).
[4] A. M. Weiner, J. P. Heritage, R. J. Hawkins, R. N. Thurston, E. M. Kirschner, D. E. Leaird, and W. J. Tomlinson, Experimental observation of the fundamental dark soliton in optical fibers, Phys. Rev. Lett. 61, 2445 (1988).
[5] M. Onorato, S. Residori, U. Bortolozzo, A. Montina, and F.

- T. Arecchi, Rogue waves and their generating mechanisms in different physical contexts, *Phys. Rep.* 528, 47 (2013).
- [6] J. M. Dudley, F. Dias, M. Erkintalo, and G. Genty, Instabilities, breathers and rogue waves in optics, *Nat. Photonics* 8, 755 (2014).
- [7] Y. S. Kivshar and G. P. Agrawal, *Optical solitons: from fibers to photonic crystals* (Academic Press, 2003).
- [8] G. P. Agrawal, *Nonlinear fiber optics* (Academic Press, New York, 2007).
- [9] P. G. Kevrekidis, D. J. Frantzeskakis, and R. Carretero-González, *Emergent nonlinear phenomena in Bose-Einstein condensates: Theory and experiment* (Springer, New York, 2008).
- [10] H. A. Haus and W. S. Wong, Solitons in optical communications, *Rev. Mod. Phys.* 68, 423 (1996).
- [11] G. D. McDonald, C. C. N. Kuhn, K. S. Hardman, S. Bennetts, P. J. Everitt, P. A. Altin, J. E. Debs, J. D. Close, and N. P. Robins, Bright solitonic matter-Wave interferometer, *Phys. Rev. Lett.* 113, 013002 (2014).
- [12] J. L. Helm, S. L. Cornish, and S. A. Gardiner, Sagnac interferometry using bright matter-Wave solitons, *Phys. Rev. Lett.* 114, 134101 (2015).
- [13] L. C. Zhao, L. Ling, Z. Y. Yang, and J. Liu, Properties of the temporal-spatial interference pattern during soliton interaction, *Nonlinear Dynam.* 83, 659 (2016).
- [14] W. Xiong, P. Gao, Z. Y. Yang, and W. L. Yang, Quantized reflection of a soliton by a vibrating atomic mirror, *Phys. Rev. A* 108, 023303 (2023).
- [15] P. Gao and J. Liu, Quantum scattering treatment on the time-domain diffraction of a matter-wave soliton, [arXiv:2311.01778](https://arxiv.org/abs/2311.01778), 2023.
- [16] N. J. Zabusky and M. D. Kruskal, Interaction of “solitons” in a collisionless plasma and the rence of initial states, *Phys. Rev. Lett.* 15, 240 (1965).
- [17] A. D. Martin, C. S. Adams, and S. A. Gardiner, Bright matter-wave soliton collisions in a harmonic trap: Regular and chaotic dynamics, *Phys. Rev. Lett.* 98, 020402 (2007).
- [18] N. N. Akhmediev, A. V. Buryak, and M. Karlsson, Radiationless optical solitons with oscillating tails, *Opt. Commun.* 110, 540 (1994).
- [19] A. V. Buryak and N. N. Akhmediev, Stability criterion for stationary bound states of solitons with radiationless oscillating tails, *Phys. Rev. E* 51, 3572 (1995).
- [20] A. Blanco-Redondo, C. Martijn de Sterke, J. E. Sipe, T. F. Krauss, B. J. Eggleton, and C. Husko, Pure-quartic solitons, *Nat. Commun.* 7, 10427 (2016).
- [21] K. K. K. Tam, T. J. Alexander, A. Blanco-Redondo, and C. M. de Sterke, Stationary and dynamical properties of pure-quartic solitons, *Opt. Lett.* 44, 3306 (2019).
- [22] V. E. Zakharov and E. A. Kuznetsov, Optical solitons and quasisolitons, *J. Exp. Theor. Phys.* 86, 1035 (1998).
- [23] K. K. K. Tam, T. J. Alexander, A. Blanco-Redondo, and C. M. de Sterke, Generalized dispersion Kerr solitons, *Phys. Rev. A* 101, 043822 (2020).
- [24] P. Gao, C. Liu, L. C. Zhao, Z. Y. Yang, and W. L. Yang, Modified linear stability analysis for quantitative dynamics of a perturbed plane wave, *Phys. Rev. E* 102, 022207 (2020).
- [25] P. Gao, L. Duan, X. Yao, Z. Y. Yang, and W. L. Yang, Controllable generation of several nonlinear waves in optical fibers with third-order dispersion, *Phys. Rev. A* 103, 023519 (2021).
- [26] A. F. J. Runge, D. D. Hudson, K. K. K. Tam, C. M. de Sterke, and A. Blanco-Redondo, The pure-quartic soliton laser, *Nat. Photonics* 14, 492 (2020).
- [27] W. H. Press, *Numerical Recipes* (Cambridge University Press, Cambridge, 1990).
- [28] T. Winiecki, J. F. McCann, and C. S. Adams, Vortex structures in dilute quantum fluids, *Europhys. Lett.* 48, 475 (1999).
- [29] M. J. Edmonds, T. Bland, D. H. J. O’Dell, and N. G. Parker, Exploring the stability and dynamics of dipolar matter-wave dark solitons, *Phys. Rev. A* 93, 063617 (2016).
- [30] J. Yang, *Nonlinear Waves in Integrable and Nonintegrable Systems* (Siam, Philadelphia, 2010).
- [31] J. M. Dudley, G. Genty, F. Dias, B. Kibler, and N. Akhmediev, Modulation instability, Akhmediev Breathers and continuous wave supercontinuum generation, *Opt. Express* 17, 21497 (2009).
- [32] L. C. Zhao and L. Ling, Quantitative relations between modulational instability and several well-known nonlinear excitations, *J. Opt. Soc. Am. B* 33, 850 (2016).
- [33] L. Duan, Z. Y. Yang, P. Gao, and W. L. Yang, Excitation conditions of several fundamental nonlinear waves on continuous-wave background, *Phys. Rev. E* 99, 012216 (2019).
- [34] G. El, A. Gurevich, V. Khodorovskii, and A. Krylov, Modulational instability and formation of a nonlinear oscillatory structure in a “focusing” medium, *Phys. Lett. A* 177, 357 (1993).
- [35] G. Biondini and D. Mantzavinos, Universal nature of the nonlinear stage of modulational instability, *Phys. Rev. Lett.* 116, 043902 (2016).
- [36] V. Achilleos, D. J. Frantzeskakis, P. G. Kevrekidis, and D. E. Pelinovsky, Matter-wave bright solitons in spin-orbit coupled Bose-Einstein condensates, *Phys. Rev. Lett.* 110, 264101 (2013).
- [37] Y. Xu, Y. Zhang, and B. Wu, Bright solitons in spin-orbit coupled Bose-Einstein condensates, *Phys. Rev. A* 87, 013614 (2013).
- [38] L. C. Zhao, X. W. Luo, and C. Zhang, Magnetic stripe soliton and localized stripe wave in spin-1 Bose-Einstein condensates, *Phys. Rev. A* 101, 023621 (2020).
- [39] Y. X. Yang, P. Gao, Z. Wu, L. C. Zhao, and Z. Y. Yang, Matter-wave stripe solitons induced by helicoidal spin-orbit coupling, *Ann. Phys.* 431, 168562 (2021).